Western University
Scholarship@Western

Chemistry Publications | Chemistry Department

2018

Polymer assembly encapsulation of lanthanide nanoparticles as contrast agents for in vivo micro-CT

Charmainne Cruje
Western University

Joy Dunmore-Buyze
Western University

Jarret P. MacDonald
Western University

David W. Holdsworth
Western University

Maria Drangova
Western University

See next page for additional authors

Follow this and additional works at: https://ir.lib.uwo.ca/chempub

 Part of the Chemistry Commons

Citation of this paper:

Cruje, Charmainne; Dunmore-Buyze, Joy; MacDonald, Jarret P.; Holdsworth, David W.; Drangova, Maria; and Gillies, Elizabeth R., "Polymer assembly encapsulation of lanthanide nanoparticles as contrast agents for in vivo micro-CT" (2018). *Chemistry Publications*. 103.
https://ir.lib.uwo.ca/chempub/103

Authors
Charmainne Cruje, Joy Dunmore-Buyze, Jarret P. MacDonald, David W. Holdsworth, Maria Drangova, and Elizabeth R. Gillies

This article is available at Scholarship@Western: https://ir.lib.uwo.ca/chempub/103

Polymer assembly encapsulation of lanthanide nanoparticles as contrast agents for *in vivo* micro-CT

Charmainne Cruje[†,‡], Joy Dunmore-Buyze[†,‡], Jarret P. MacDonald[§], David W. Holdsworth[†,‡], Maria Drangova[†,‡], Elizabeth R. Gillies[,§,||]*

[†]Department of Medical Biophysics, [‡]Robarts Research Institute, [§]Department of Chemistry, and [||]Department of Chemical and Biochemical Engineering, The University of Western Ontario, 1151 Richmond Street, London, Ontario N6A 5B7, Canada

ABSTRACT

Despite recent technological advancements in microcomputed tomography (micro-CT) and contrast agent development, pre-clinical contrast agents are still predominantly iodine-based. Higher contrast can be achieved when using elements with higher atomic numbers, such as lanthanides; lanthanides also have x-ray attenuation properties that are ideal for spectral CT. However, the formulation of lanthanide-based contrast agents at the high concentrations required for vascular imaging presents a significant challenge. In this work, we developed an erbium-based contrast agent that meets micro-CT imaging requirements, which include colloidal stability upon redispersion at high concentrations, evasion of rapid renal clearance, and circulation times of tens of minutes in small animals. Through systematic studies with poly(ethylene glycol) (PEG)-poly(propylene glycol), PEG-polycaprolactone, and PEG-poly(L-lactide) (PLA) block

copolymers, the amphiphilic block copolymer PEG_{114}-PLA_{53} was identified to be ideal for encapsulating oleate-coated lanthanide-based nanoparticles for *in vivo* intravenous administration. We were able to synthesize a contrast agent containing 100 mg/mL of erbium that could be redispersed into colloidally stable nanoparticles in saline after lyophilization. Contrast enhancement of over 250 HU was achieved in the blood pool for up to an hour, thereby meeting the requirements of live animal micro-CT.

KEYWORDS

contrast agent, lanthanides, nanoparticles, micro-CT, polymer self-assembly

INTRODUCTION

With the ultimate goal of developing methods to treat human disease, small animal models are used extensively in cardiovascular, orthopedic, and cancer research.[1-3] The advantages of using small animals include short gestation times, low maintenance costs and ease of genetic manipulation.[4] In order to study disease at scales suitable for small animals, high-resolution imaging techniques (i.e., micro-imaging) have been developed; these include micro magnetic resonance imaging,[5, 6] micro positron emission tomography,[7] micro-ultrasound,[8, 9] and micro computed tomography (micro-CT).[10] Among these, micro-CT has been the most utilized, based on scientific publications in the last five years.

Micro-CT's ubiquity is attributable to the fact that the modality is quantitative, three-dimensional, non-destructive, fast and cost-effective. Contrast in micro-CT is derived from the differential attenuation of x-rays by various tissues. Unfortunately, soft tissues, which have similar

densities, have little differential CT contrast and exogenous agents are required to provide contrast. For example, to image the vasculature, x-ray attenuating contrast agents are injected intravenously to "opacify" the vessels during the acquisition of the micro-CT scan. With these contrast agents, vascular imaging by micro-CT can potentially be utilized to reliably track the development of blood vessels during the process of angiogenesis and in studying the effect of novel therapies for re-vascularization.[11] For human imaging, CT contrast agents are typically small iodinated molecules, which are cleared within a few minutes through the renal system. However, micro-CT scan times can be as long as tens of minutes and successful imaging of the vasculature requires the use of contrast agents that clear from the blood over extended time periods. These agents are referred to as "blood pool" contrast agents.

Several CT blood pool contrast agents are available commercially for *in vivo* small animal research.[12, 13] These have been made possible by advances in nanotechnology and consist of particles large enough to evade immediate renal clearance (i.e. > 10 nm).[14] Initially, commercially available nanoparticle-based blood-pool contrast agents were iodine-based to take advantage of the strong attenuation of iodine at low energies (k-edge = 33.2 kEv) and included Fenestra VC (containing 50 mg/mL of iodine) and eXia 160 XL (containing 160 mg/mL of iodine).[13, 15] More recently gold-based agents have been developed (e.g. AuroVist 15 nm, containing 200 mg/mL of gold), which take advantage of the high density of gold.[16] These agents have been developed with the intent to deliver a high loading of metal (x-ray attenuator) in a small volume of contrast agent and thereby to provide higher contrast between the vessels and surrounding tissue.

Another class of metals appropriate for CT contrast agents is the lanthanides. These elements are of particular interest because they have k-edges near the average energies used in micro-CT (between 80 kVp and 120 kVp). This property makes the lanthanides ideally suited to use with

specialized micro-CT techniques that take advantage of the spectral properties of materials, such as dual-energy imaging and spectral CT. Of the lanthanides, gadolinium has been used most extensively as a contrast agent for magnetic resonance imaging (MRI). Polymer particles decorated with gadolinium, such as the chelated derivative of diethylenetriaminepentaacetic acid and Gd(III) on a cross linked polymer nanogel, have been synthesized and used for vessel imaging of mice, but have Gd loading that is too low for CT imaging (typically < 0.5 mg/mL).[17-19]

Lanthanide-based nanoparticles have also been explored for imaging, largely due to their abilities to alter proton relaxation times in MRI in the case of gadolinium[20, 21] or their photon upconversion capabilities in the case of $NaLnF_4$ (where Ln is a lanthanide and the system is co-doped).[22-24] However, such particles are usually synthesized with hydrophobic ligands,[25] making it challenging to disperse them with high stability in blood. Chatterjee et al. achieved this by coating lanthanide-based nanoparticles with polyethyleneimine, reaching concentrations of 4.4 mg/mL (used subcutaneously for upconversion luminescence imaging).[22] Budijono et al. explored the encapsulation of lanthanide-based nanoparticles in block copolymer assemblies, and demonstrated the stability of these assemblies in serum media at low concentrations (< 1 mg/mL).[24] Similary, Zhu et al. used pH-responsive block copolymers to encapsulate gadolinium-based nanoparticles, and demonstrated that they could stabilize the nanoparticles in aqueous solution at low concentrations (< 0.1 mg/mL).[21] However, to date only Liu et al., have synthesized a lanthanide contrast agent with a concentration high enough for micro-CT imaging.[26] They encapsulated 70 mg/mL of ytterbium in 1,2-distearoyl-sn-glycero-3-phosphoethanolamine-terminated poly(ethylene glycol) (PEG) and demonstrated circulation in the blood pool for approximately 20 minutes. However, even higher lanthanide concentrations and blood circulation times are required for high resolution imaging of the vasculature.

In this study, we present a simple and systematic method to prepare a lanthanide-based contrast agent for micro-CT applications, which require high contrast-element loading (> 100 mg/mL preferred) and long circulation times (ideally > 30 minutes). The high lanthanide concentration poses a significant challenge, particularly when paired with the need to add polymers, which are required to achieve long circulation times. Erbium, which we have demonstrated to be an excellent contrast agent for *ex vivo* imaging, was selected as the lanthanide.[27] Oleate-coated $NaErF_4$ nanoparticles (ErNP) were synthesized and encapsulated into core-shell nanoassemblies via nanoprecipitation using a series of amphiphilic block copolymers (Figure 1). A sequence of optimization steps was then performed to identify an ideal polymer, which encapsulates a high lanthanide content while remaining colloidally stable after redispersion in saline and a mouse-blood mimic. Once the ideal polymer was identified, the lanthanide-based contrast agent was evaluated *in vivo* over a period of one hour. To our knowledge, this is the first demonstration of the successful synthesis of an *in vivo* lanthanide-based blood pool agent that can be dispsersed into colloidally stable assemblies containing 100 mg/mL of erbium.

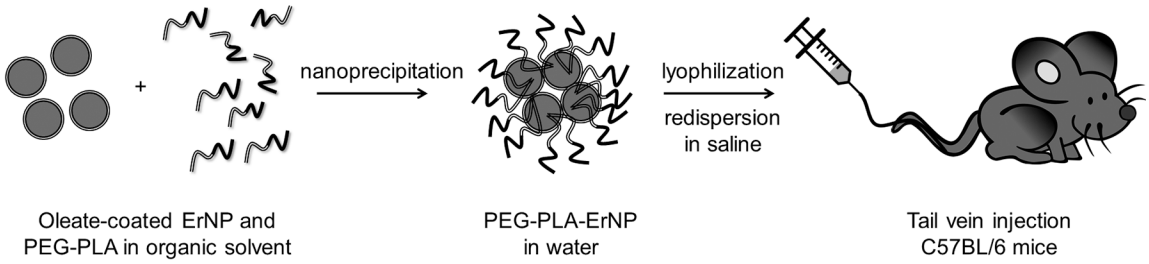

Figure 1. Schematic representation of self-assembled erbium-based nanoparticles as a pre-clinical blood pool contrast agent.

EXPERIMENTAL SECTION

Materials and General Methods

Reagents were purchased from commercial suppliers as described in the Supporting Information (SI) and were used without further purification unless otherwise noted. Methods used in the synthesis and characterization of the materials are also presented in the SI document.

Nanoprecipitation for self-assembly of polymeric nanoparticles containing erbium nanoparticles

Erbium nanoparticles (ErNP) were synthesized by a previously reported method.[28, 29] The ErNP were self-assembled with purchased poly(ethylene glycol) (PEG)-poly(propylene glycol) (PPG) triblock copolymers (PEG_{76}-PPG_{22}-PEG_{76} and PEG_{137}-PPG_{34}-PEG_{137} where the subscripts indicate the degree of polymerization of the blocks), or synthesized diblock copolymers of PEG-poly(ε-caprolactone)(PCL) (PEG_{45}-PCL_{20}, PEG_{45}-PCL_{51}, PEG_{114}-PCL_{51}, PEG_{114}-PCL_{97}) or PEG-poly(l-lactide) (PEG_{45}-PLA_{25}, PEG_{45}-PLA_{52}, PEG_{114}-PLA_{53}, PEG_{114}-PLA_{122}).[30, 31] ErNP (2 mg) were dissolved in 0.1 mL of tetrahydrofuran (THF). Separately, 8 mg of copolymer was dissolved in 0.1 mL of THF. These solutions were then combined and added dropwise to 1.8 mL of deionized water under magnetic stirring. After 1 hour, stirring was stopped and the solution was left uncapped for 12 hours to allow for organic solvent evaporation. The solutions were then dialyzed against 100 mL of deionized water for 2 days with 5 solvent changes. A 450 nm syringe filter was used to remove large aggregates and the samples were characterized by dynamic light scattering (DLS), transmission electron microscopy (TEM) and inductively coupled plasma mass spectrometry (ICP-MS).

Colloidal stability of the polymeric nanoparticles

The sterile polymeric nanoparticles containing ErNP were lyophilized prior to redispersion in saline. Saline is used as the solvent of the NPs prior to intravenous injection *in vivo* because it is isotonic with blood. Therefore the particles must remain colloidally stable in that environment. DLS size measurements were performed on the redispersed ErNP and the average sizes of the samples were observed for up to one hour.

Varying the polymer content of the nanoparticles

The polymeric nanoparticles containing ErNP that remained colloidally stable after freeze-drying and redispersion in saline, and that encapsulated relatively higher erbium amounts were selected (PEG_{114}-PLA_{53}). Solutions with varying mass ratios were prepared. Synthesized ErNP (80 mg dissolved in 4 mL of THF) were added to 320, 160, 80 or 40 mg of PEG_{114}-PLA_{53} in 4 mL of THF. These solutions were combined and added dropwise to 100 mL of deionized water under magnetic stirring. After 1 hour, stirring was stopped and the suspension was left uncapped for 12 hours to allow for organic solvent evaporation. The suspensions were then dialyzed against 500 mL of deionized water for 2 days with 5 solvent changes. A 450 nm syringe filter was used to remove large aggregates and the samples were characterized by DLS, TEM and ICP-MS. The samples were lyophilized, sterilized and re-dispersed in 400 μL of saline. 10 μL of the samples were added to 990 μL of saline or mouse serum mimic for an hour-long time-course DLS study. The mouse serum mimic was pH 7.4 phosphate buffered saline containing 0.5 μg/mL mouse immunoglobulins, 1 wt% bovine serum albumin and 0.1 wt% sodium azide. Colloidal stability in a mouse serum mimic *in vitro* will serve as an indicator of its stability *in vivo*. An increase in the

average size signifies aggregation, which would lead to immune system detection followed by clearance from the blood pool *in vivo*.

General micro-CT imaging and analysis methods

Micro-CT images were acquired using the GE Locus Ultra (London, ON) with a protocol previously used to evaluate contrast agent distribution *in vivo*.[15, 32] Briefly, 1000 views (16 ms per view) were acquired at 80 kVp, 55 mA over 360° and reconstructed using a cone-beam reconstruction algorithm. The resulting images have a voxel size of 150 × 150 × 150 μm. Images were analyzed using MicroView (Parallax Innovations, London, ON) and CT contrast was reported in Hounsfield Units (HU – a standard linear scale of x-ray attenuation coefficient, where air = -1000 HU and water = 0 HU). All HU values were measured over a volume of 450 × 450 × 150 μm.

Micro-CT imaging of erbium-containing polymeric nanoparticles

The relationship between CT contrast and erbium concentration was first determined by micro-CT. Erbium chloride was diluted in saline at erbium concentrations of 5, 10, 20 and 100 mg/mL, which acted as calibration standards. The linear regression between CT contrast (in HU) and erbium concentration was then used to measure the erbium concentrations resulting when 40 mg of each of the lyophilized 1:1 and 0.5:1 PEG_{114}-PLA_{53}:ErNP formulations were separately dispersed in 0.2 mL of saline.

Toxicity of the contrast agent

The 1:1 and 0.5:1 PEG_{114}-PLA_{53}:ErNP mass ratio formulations were tested. Details of these experiments are described in the SI document. Briefly, an *in vitro* cell viability assay was done using C2C12 mouse myoblast cells from Millipore Sigma (Oakville, ON). The cells were incubated with the contrast agent for 24 hours, after which cell viability was measured using a 3-(4,5- dimethylthiazol-2-yl)-2,5-diphenyltetrazolium bromide (MTT) assay.

Following *in vitro* tests, the *in vivo* toxicity of the contrast agent was evaluated using the dorsal interscapular subcutaneous tissue of C57BL/6 male mice (25-30 g). All animal studies were carried out in accordance with the regulations set out by the University of Western Ontario's Council on Animal Care, in agreement with the ARRIVE guidelines, and were carried out in accordance with the U.K. Animals Act, 1986 and associated guidelines.

Intravenous administration of the contrast agent and characterization of distribution *in vivo*

Five C57BL/6 male mice (25-30 g) were anesthetized initially with 4% isoflurane, and then 1.5% for maintenance, in O_2 via a nose cone placed on the snouts of the animals. The tail veins were catheterized using PE-20 polyethylene tubing. For each mouse, images were first acquired prior to contrast administration. The contrast agent (0.2 mL) was injected over a period of 3 minutes and three scans were acquired, starting 2 minutes following the end of injection and ending 60 minutes post injection. The 1:1 PEG_{114}-PLA_{53}:ErNP (mass ratio) was tested in 3 mice and the 0.5:1 mass ratio formulation was evaluated in 2 mice.

RESULTS AND DISCUSSION

Synthesis and characterization of oleate-coated ErNP

$NaErF_4$ nanoparticles were synthesized based on a previously reported method.[28, 29] DLS measurements of ErNP in THF reported a Z-average diameter of 50 ± 1 nm and a polydispersity index (PDI) of 0.18 ± 0.02 (Figure 2a and Figure S2). These results were supported by TEM imaging (Figure 2b).

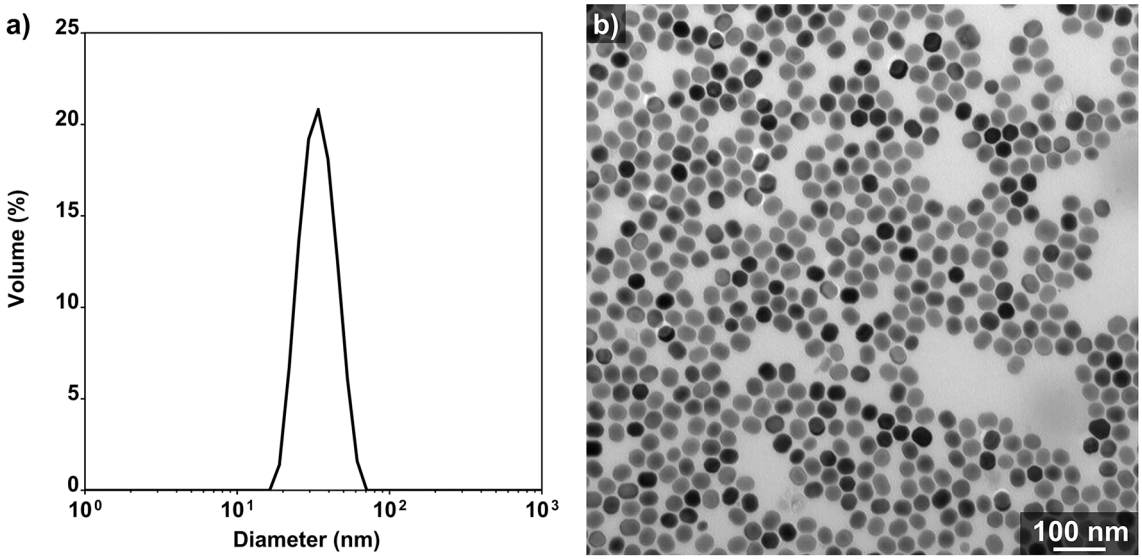

Figure 2. a) Volume diameter distribution of ErNP in THF measured by DLS. b) A TEM image of the oleate-coated ErNP.

Synthesis and characterization of diblock copolymers

The ErNP are oleate-coated, which makes them incompatible with the aqueous blood pool.[33] It was envisioned that by nanoprecipitation of the ErNP with amphiphilic block copolymers, assemblies containing hydrophobic ErNP in the hydrophobic polymer cores and hydrophilic stabilizing polymer coronas would be formed (Figure 1). Polymers are relatively easy to prepare, are colloidally stable even at low concentration, and can be synthesized at different lengths using various monomers, making them tunable and versatile materials.[34] We used PEG as the hydrophilic

block for its well-known stealth properties against the immune system.[35, 36] In lieu of displacing the oleate on the ErNP surface with polymers,[29, 37] we chose to synthesize polymeric micelles by nanoprecipitation, which is a fast, reproducible, and cost-effective means of suspending hydrophobic cargo in polar solvents.[38] Displacing the oleate on the ErNP surface would favor the suspension of individual nanoparticles in solution, which is not a requirement in micro-CT.

To identify a carrier that would encapsulate high erbium content while surviving lyophilization and redispersion in saline, a series of amphiphilic block copolymers was studied (Figure 3, Table 1). Two PEG-PPG-PEG triblock copolymers (commonly referred to as poloxamers), which are commercially available, cost-effective and are FDA-approved for intravenous administration in humans, were used to form the polymeric assemblies.[39] In addition, several block lengths of PEG-PCL and PEG-PLA were synthesized and studied. These diblock copolymers were selected because they are used clinically as therapeutic drug carriers and are also currently in further clinical trials.[40] The characteristics of the polymeric micelles may change upon varying the copolymer's properties (i.e. hydrophobicity of the non-polar block, total block length, and PEG ratio).[41]

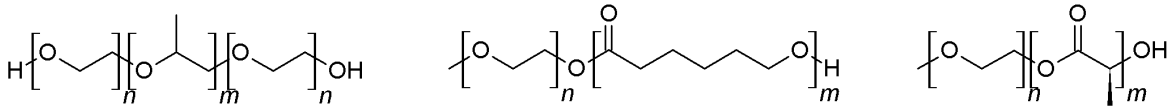

Figure 3. Chemical structures of the amphiphilic block copolymers that were used to form the polymeric assemblies.

Table 1. SEC and ^{1}H NMR characterization results of diblock copolymers. [a]Determined by ^{1}H NMR spectroscopy; [b]Determined by SEC.

Copolymer	PEG molar mass (g/mol)	Monomer feed (equiv.)	PCL or PLA molar mass[a]	M_n[a]	M_n[b]	$Đ$[b]	f value[a]
PEG_{76}-PPG_{22}-PEG_{76}	6700	-	-	8400	-	-	0.80
PEG_{137}-PPG_{34}-PEG_{137}	12000	-	-	14600	-	-	0.82
PEG_{45}-PCL_{20}	2000	18	2300	4300	5600	1.1	0.47
PEG_{45}-PCL_{51}	2000	35	5800	7800	6300	1.4	0.26
PEG_{114}-PCL_{51}	5000	44	5900	10900	9500	1.1	0.46
PEG_{114}-PCL_{97}	5000	88	11100	16100	10300	1.3	0.31
PEG_{45}-PLA_{25}	2000	22	2300	4300	5200	1.2	0.47
PEG_{45}-PLA_{52}	2000	44	4700	6700	9600	1.1	0.30
PEG_{114}-PLA_{53}	5000	56	4800	9800	10500	1.3	0.51
PEG_{114}-PLA_{122}	5000	111	11000	16000	13500	1.4	0.31

PEG-PCL and PEG-PLA were synthesized using PEG monomethyl ether (2000 or 5000 g/mol) as the initiator and the block ratios were tuned by varying the equivalents of ε-caprolactone or L-lactide to achieve PEG mass fractions (f) of approximately 0.5 and 0.3. Methanesulfonic acid was used as the polymerization catalyst for the synthesis of PEG-PCL, while 1,5,7-triazabicyclo[4.4.0]dec-5-ene was used as the catalyst for PEG-PLA synthesis.[30, 31] A 1:1 ratio of catalyst:initiator was used in each case. Characterization of the diblock copolymers was performed using ^{1}H nuclear magnetic resonance (NMR) spectroscopy (Figures S3-S10) and size exclusion chromatography (SEC) relative to polystyrene standards (Figures S11-S14) and the results are summarized in Table 1. Typical signals of PEG, PCL and PLA components were utilized to calculate the molar ratios of polymerized monomers to PEG and thus the number average

molecular weight (M_n). The M_n and molar mass dispersities ($Đ$) were also measured by SEC. The f values were calculated from the NMR data, as this should provide the most accurate assessment of the block ratios. The values indicated for the poloxamers were taken from their respective specification sheets. Overall, the measured M_n values, particularly from NMR spectroscopy, and f values were in good agreement with the target structures.

Polymer self-assembly and ErNP encapsulation

First, the self-assembly of the block copolymers without ErNPs was investigated. The copolymers were dissolved in THF then this solution was added to water with stirring. After removal of THF by dialysis, the resulting nanoassemblies were characterized by DLS and TEM. The Z-average diameters measured by DLS ranged from 11 to 55 nm (Table 2, Figure S15), consistent with self-assembly into micelles and TEM images confirmed that solid spherical particles were formed (Figure S16). The PDIs ranged from 0.1 to 0.6, suggesting that some copolymers assembled into reasonably monodisperse nanoparticles (PDI < 0.3), whereas others exhibited a large distribution of sizes (PDI > 0.3). In general, the TEM results were in good agreement with the volume distributions obtained from DLS, except for both poloxamers (PEG_{76}-PPG_{22}-PEG_{76} and PEG_{137}-PPG_{34}-PEG_{137}). For these poloxamers, the volume distribution in DLS suggested the presence of small scatterers that could be unassembled copolymers in solution, whereas the corresponding TEM images showed larger nanoparticles that could result from aggregation during the drying process.

Table 2. Z-average diameters and PDIs obtained using DLS for the self-assembly of block copolymers without ErNP. Each assembly was prepared and measured in triplicate and the error measurements correspond to the standard deviations on these batches.

Polymer	Z-average diameter (nm)	PDI
PEG_{76}-PPG_{22}-PEG_{76}	11 ± 2	0.6 ± 0.3
PEG_{137}-PPG_{34}-PEG_{137}	17 ± 3	1.0 ± 0.4
PEG_{45}-PCL_{20}	20 ± 1	0.2 ± 0.1
PEG_{45}-PCL_{51}	17 ± 2	0.1 ± 0.1
PEG_{114}-PCL_{51}	18 ± 4	0.1 ± 0.1
PEG_{114}-PCL_{97}	31 ± 4	0.2 ± 0.1
PEG_{45}-PLA_{25}	26 ± 11	0.5 ± 0.2
PEG_{45}-PLA_{52}	29 ± 8	0.4 ± 0.1
PEG_{114}-PLA_{122}	31 ± 10	0.4 ± 0.2
PEG_{114}-PLA_{53}	55 ± 8	0.2 ± 0.1

Having confirmed the self-assembly behavior of the amphiphilic block copolymers alone, ErNPs were then added. Both the copolymer and ErNP were dissolved in THF and then nanoprecipitated into water to form suspensions of erbium-containing assemblies. The mass ratio of polymer:ErNP was 4:1. THF was removed by dialysis, then the suspensions were passed through a 0.45 μm filter. This filtration served to remove any ErNP that had not been encapsulated and consequently aggregated, as well as polymer-ErNP assemblies that were too large and would be preferentially cleared from the blood by the mononuclear phagocytic system (MPS).[42,43] The resulting assemblies were characterized by DLS and TEM (Figure 4, Table 3). The TEM images showed individual

ErNP or groups of ErNP across the grid, unlike the oleate-coated ones in Figure 2b, which displayed no specific organization or aggregation. This suggests the encapsulation of the ErNP within the amphiphilic block copolymers. It should be noted that the polymers were indiscernible in the TEM images because of the high contrast from the ErNP. The Z-average diameters that were measured by DLS ranged from 53 to 183 nm. This also supported the encapsulation of ErNP within the amphiphilic block copolymers, as these diameters were larger than those of the polymer-only micelles.

When PEG_{114}-PLA_{122} or any of the PEG-PCL diblock copolymers were used to form the assemblies, moderate PDIs (between 0.2 and 0.3) were observed. On the other hand, when using either poloxamers or the other PEG-PLA diblock copolymers good PDIs (< 0.2) were obtained. Because the contrast agent was simply required to remain in circulation (i.e. no tissue-targeting was required), obtaining low PDIs was not of utmost importance; meeting the size requirements that would allow evasion of immediate renal clearance and preferential uptake by the MPS was sufficient.

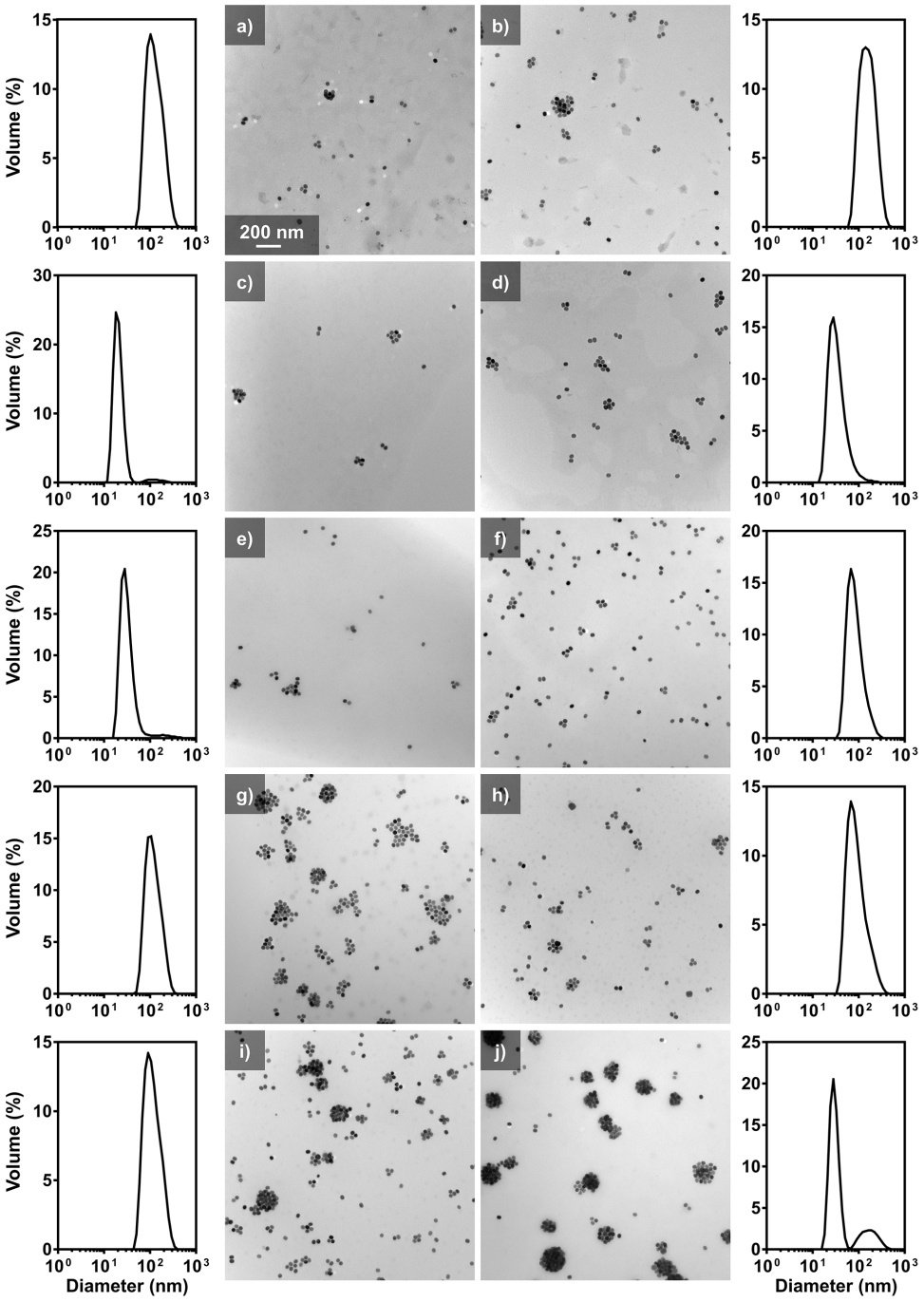

Figure 4. DLS volume (%) diameter distributions and the corresponding TEM images of polymer-encapsulated ErNP using a) PEG_{76}-PPG_{22}-PEG_{76}, b) PEG_{137}-PPG_{34}-PEG_{137}, c) PEG_{45}-PCL_{20}, d) PEG_{45}-PCL_{51}, e) PEG_{114}-PCL_{51}, f) PEG_{114}-PCL_{97}, g) PEG_{45}-PLA_{25}, h) PEG_{45}-PLA_{52}, i) PEG_{114}-PLA_{53}, and j) PEG_{114}-PLA_{122}.

Table 3. Characterization data for the polymer-encapsulated ErNP obtained from DLS and ICP-MS both as initially prepared and after lyophilization followed by resuspension in saline. The polymer:ErNP mass ratios were 4:1 unless otherwise indicated. Each assembly was prepared and measured in triplicate and the error measurements correspond to the standard deviations on these batches. [a]Determined by DLS; [b]Determined by ICP-MS where 780 μg/L would correspond to encapsulation of 100% of the Er added during self-assembly.

Polymer	In water following initial preparation[a]		Post-lyophilization and resuspension in saline[a]		Erbium content (μg/L)[b]
	Z-average (nm)	PDI	Z-average (nm)	PDI	
PEG_{76}-PPG_{22}-PEG_{76}	174 ± 4	0.1 ± 0.1	294 ± 34	0.2 ± 0.1	62 ± 6
PEG_{137}-PPG_{34}-PEG_{137}	176 ± 6	0.1 ± 0.1	212 ± 2	0.2 ± 0.1	232 ± 1
PEG_{45}-PCL_{20}	98 ± 10	0.3 ± 0.1	2145 ± 179	0.2 ± 0.1	377 ± 25
PEG_{45}-PCL_{51}	82 ± 2	0.3 ± 0.1	3204 ± 416	0.2 ± 0.1	506 ± 3
PEG_{114}-PCL_{51}	53 ± 5	0.3 ± 0.1	1057 ± 32	0.6 ± 0.1	596 ± 21
PEG_{114}-PCL_{97}	84 ± 1	0.2 ± 0.1	2861 ± 9	0.4 ± 0.5	732 ± 22
PEG_{45}-PLA_{25}	165 ± 2	0.1 ± 0.1	192 ± 4	0.5 ± 0.1	407 ± 2
PEG_{45}-PLA_{52}	151 ± 2	0.2 ± 0.1	1597 ± 83	0.4 ± 0.1	149 ± 1
PEG_{114}-PLA_{122}	130 ± 2	0.2 ± 0.1	301 ± 13	0.4 ± 0.1	339 ± 4
PEG_{114}-PLA_{53}	154 ± 2	0.1 ± 0.1	134 ± 1	0.2 ± 0.1	599 ± 3
PEG_{114}-PLA_{53} (2:1)	180 ± 3	0.2 ± 0.1	180 ± 6	0.1 ± 0.1	583 ± 28
PEG_{114}-PLA_{53} (1:1)	179 ± 4	0.2 ± 0.1	171 ± 3	0.2 ± 0.1	607 ± 16
PEG_{114}-PLA_{53} (0.5:1)	183 ± 3	0.1 ± 0.1	185 ± 5	0.2 ± 0.1	533 ± 32

Redispersion and characterization of the lyophilized polymer-encapsulated ErNP

Because the polymer-encapsulated ErNP were prepared by nanoprecipitation at low concentrations in water, the sample had to be lyophilized then redispersed at higher concentrations. The ability to lyophilize and resuspend the assemblies is also advantageous for their long-term storage. Dried samples were redispersed in 0.9% saline, which is isotonic with blood, and the Z-average diameters of the assemblies were measured by DLS (Table 3). No filtration was performed after redispersion. In addition, because colloidal stability of the contrast agent in its administration medium is required, the Z-average diameters of the redispersed ErNP-loaded assemblies were also observed by DLS over 60 minutes.

Relative to the pre-lyophilized diameters, minimal changes occurred for the PEG_{137}-PPG_{34}-PEG_{137}, PEG_{45}-PLA_{25}, and PEG_{114}-PLA_{53} assemblies, while the remainder redispersed in saline at much larger hydrodynamic diameters, suggesting that they were aggregated. For example, the PEG_{76}-PPG_{22}-PEG_{76} assemblies, which initially had a Z-average hydrodynamic diameter of 174 ± 4 nm had a diameter of 294 ± 34 nm after redispersion in saline, while the PEG_{137}-PPG_{34}-PEG_{137} assemblies, which were initially 176 ± 6 nm, were redispersed in saline at 212 ± 2 nm (Figure S17). Given the very similar f values for these polymers, the larger PEG block is likely capable or better stabilizing the particles. All PEG-PCL assemblies redispersed in saline as micrometer-sized particles, which was undesirable, as these particles would be rapidly cleared by the MPS (Figure S18). The colloidal instabilities of PEG-PCL assemblies may result from PCL's high hydrophobicity or crystallinity. The PEG_{45}-PLA_{52} assemblies also redispersed as microparticles and PEG_{114}-PLA_{122} assemblies redispersed at an increased Z-average diameter of 301 ± 13 nm compared to an initial diameter of 130 ± 2 nm (Figure S19). Both of these copolymers had low f values of ~0.3, which may contribute to their poor stability to redispersion. However, PEG_{45}-PLA_{25}

and PEG_{114}-PLA_{53} assemblies retained Z-average diameters of 192 ± 4 and 134 ± 1 nm after redispersion in saline, similar to their initial diameters of 165 ± 2 and 154 ± 2 nm. Both remained colloidally stable for up to 60 minutes. This stability may result from their increased f values of ~0.5.

ICP-MS was used to quantify the concentration of erbium that was encapsulated by each system (Table 3). These measurements were performed on the initially prepared samples after their filtration. If all of the added erbium had remained dispersed in assemblies less than 0.45 μm in diameter, the expected erbium concentration of the suspensions would have been 780 μg/L. The highest erbium content was observed for PEG_{114}-PCL_{97} at 732 ± 22 μg/L. The second highest concentration was obtained with PEG_{114}-PLA_{53} at 599 ± 3 μg/L, then PEG_{114}-PCL_{51} at 596 ± 21 μg/L. However, out of the assemblies formed by these block copolymers, only PEG_{114}-PLA_{53} assemblies could be redispersed without a substantial increase in Z-average diameter in saline. The other block copolymers that allowed size consistency had lower erbium content, with PEG_{137}-PPG_{34}-PEG_{137} at 232 ± 1 ug/L and PEG_{45}-PLA_{25} at 407 ± 2 μg/L. Decreased erbium content resulted from the filtration of unencapsulated hydrophobic ErNP that aggregated in water or ErNP in assemblies larger than 0.45 μm in diameter. Based on this analysis, further studies were performed with PEG_{114}-PLA_{53} as it was able to form stable assemblies with high erbium content.

Characterization of the assemblies formed with PEG_{114}-PLA_{53}

The polymer content of the contrast agent does not contribute to the attenuation of x-rays and hence will not contribute to higher contrast. It does however contribute to the total mass of the material in solution, and increases viscosity, thereby making administration of the suspension difficult. Thus, it would be desirable to decrease the polymer:ErNP ratio in the assemblies.

However, decreasing the polymer content of the assemblies has one drawback, which is the potential decrease of their stealthiness and immune system evasion.[36] To investigate the possibility of lowering the polymer content of the contrast agent while retaining stability, assemblies were formed with lower PEG_{114}-PLA_{53}:ErNP mass ratios (from 4:1 to 2:1, 1:1 and 0.5:1). Their colloidal stabilities at 37 °C in saline and in a mouse serum mimic were studied by DLS (Figure 5). The serum mimic contained bovine serum albumin and ions at concentrations that are similar to mouse blood. The proteins can potentially contribute to polymer shedding, and thereby to nanoparticle aggregation *in vitro*. In the blood pool of the animal *in vivo*, polymer shedding leads to the detection by the immune system and clearance of the nanoparticles from the blood via the liver.[35, 36] In the DLS analysis, the proteins generated insignificant scattering that did not interfere with the analysis of the assemblies (Figure S20-S21). The Z-average diameters for the initially prepared assemblies ranged from 121-185 nm and did not vary significantly over a period of 60 minutes in saline or in the mouse blood mimic, indicating that each formulation was sufficiently stable.

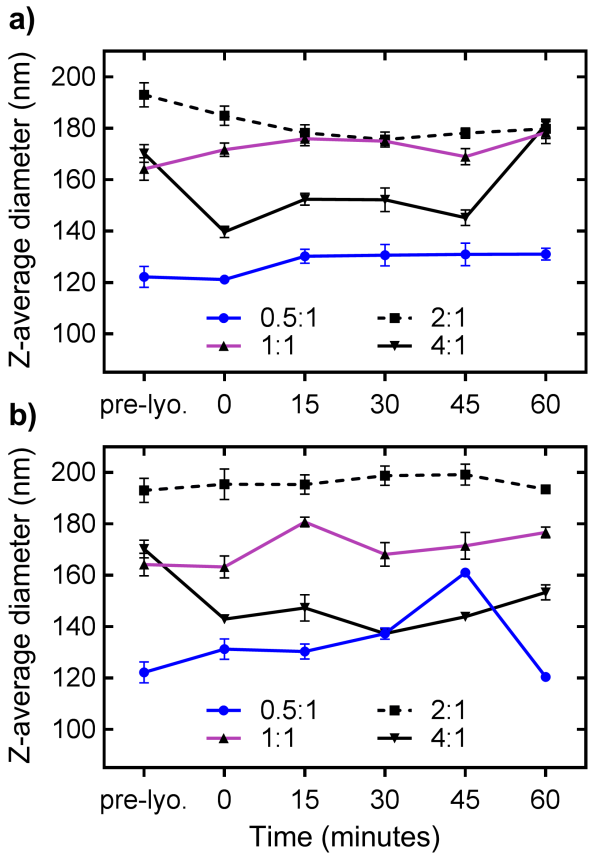

Figure 5. Time-course DLS results at 37 °C for PEG_{114}-PLA_{53}-encapsulated ErNP post-lyophilization after redispersion in a) saline and b) mouse serum mimic.

TEM imaging of the assemblies and analyses of their erbium content were also performed. Denser ErNP cores were observed when the polymer:ErNP ratio was reduced (Figure 6). Thus, decreasing the availability of polymers favored higher ErNP loading per assembly. ICP-MS results revealed similar erbium content in the suspensions for all of the mass ratios. Given this, and their colloidal stability *in vitro*, all the formulations should demonstrate similar contrast enhancement values over time once concentrated and administered to the blood pool. However, the concentrated solutions formed with polymer:ErNP mass ratios of 4:1 and 2:1 had high viscosities that made the

solutions too challenging to administer *in vivo* though the 30 G needles. Hence, for subsequent studies, the assemblies containing PEG_{114}-PLA_{53}:ErNP mass ratios of 1:1 and 0.5:1 were used. Using pyrene as a fluorescent probe,[44] the critical aggregation concentrations (CACs) for these 1:1 and 0.5:1 formulations were measured and compared to that of PEG_{114}-PLA_{53} assemblies without ErNP. We found that the CAC of the block copolymer alone was 26 mg/L, whereas those of the 1:1 and 0.5:1 PEG_{114}-PLA_{53}:ErNP formulations were 96 mg/L and 117 mg/L respectively (Figures S22-S24). Thus, it is evident that the loading of ErNP destabilizes the assemblies to some extent. Nevertheless, these CAC values are much lower than the concentrations at which they would be administered, even after dilution into the blood pool.

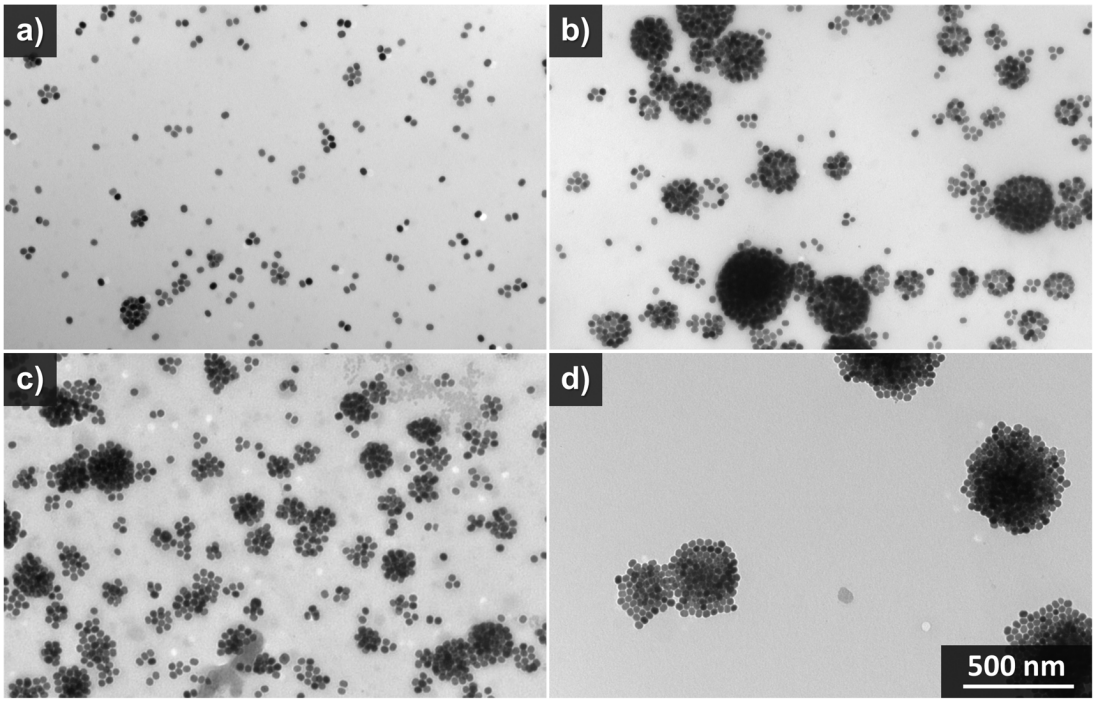

Figure 6. TEM images of the PEG114-PLA53-encapsulated ErNP using polymer:ErNP mass ratios of a) 4:1, b) 2:1, c) 1:1, d) 0.5:1.

Erbium content in ErNP determined via Micro-CT

While ICP-MS was used to detect erbium content before lyophilization, micro-CT was used to confirm the erbium content of the redispersed and high concentration versions of the contrast agents. A linear relationship between an element's concentration and its attenuation of x-rays exists and does not depend on the specific chemical form of the element. This quantitative property of micro-CT contrast is one of its advantages as an imaging modality. Calibration standards containing erbium chloride dissolved in saline at concentrations of 0, 5, 10, 20 and 100 mg/mL of erbium were scanned. Using linear regression of the measured CT numbers of the standards (Figure S25), it was determined that 40 mg of the lyophilized 1:1 and 0.5:1 PEG_{114}-PLA_{53}:ErNP formulations dispersed in 0.2 mL of saline resulted in contrast element concentrations of 48 and 74 mg/mL of erbium respectively. Therefore, 100 mg/mL is achieved when 42 mg of the 1:1 formulation and 27 mg of the 0.5:1 formulation is suspended in 0.1 mL of saline. Micro-CT scans of the high concentration suspensions verified that 100 mg/mL of erbium was achieved when the calculated amount of the agent was used (Figure S26). While higher erbium loading can be achieved with more concentrated solutions, we restricted the experiments to 100 mg/mL in order to maintain low viscosities for intravenous injection in mice.

Toxicity of the contrast agent

The *in vitro* and *in vivo* toxicity of the contrast agent was evaluated prior to its intravenous administration. Based on MTT assays, greater than 80% viability relative to controls was observed for the 1:1 polymer to erbium mass ratio formulation up to concentrations of 0.5 mg/mL (Figure S27). The 0.5:1 polymer to erbium formulation was even less toxic, with greater than 80% viability up to 1 mg/mL, the highest concentration tested. We also performed subcutaneous injections to

study the materials *in vivo*. Subcutaneous tissue has slow absorption and clearance rates of exogenous materials, which provides an opportunity to study the reaction of tissues to the contrast agent over prolonged periods. Three-dimensional micro-CT images were obtained in mice before the subcutaneous injection of the 1:1 and 0.5:1 PEG_{114}-PLA_{53}:ErNP formulations and two weeks after the administration of the agent. Each scan took 16 seconds to acquire. Representative micro-CT images for each of the contrast agent formulation injections are shown in Figure S28. The images show that the contrast agent localized near the injection site for up to two weeks. Gross examination of the subcutaneous tissue confirmed the presence of some contrast agent near the injection site. No abnormalities were observed in either the subcutaneous tissue or the dermis (Figure S29).

Distribution of the contrast agent *in vivo*

Three-dimensional micro-CT images were obtained in mice before the intravenous administration of both contrast agent formulations and at three time points following the administration of the agent. Each scan took 16 seconds to acquire. Representative micro-CT images for each of the contrast agents are shown in Figure 7. After contrast agent administration, all the major vessels – particularly the external jugular and axillary veins in Figure 7 – became clearly visible. For both formulations, there appeared to be no change in contrast in the chambers of the heart for up to 60 minutes. The contrast in the liver was seen as early as the 2-minute time point – demonstrated by the ability to distinguish liver from surrounding soft tissue.

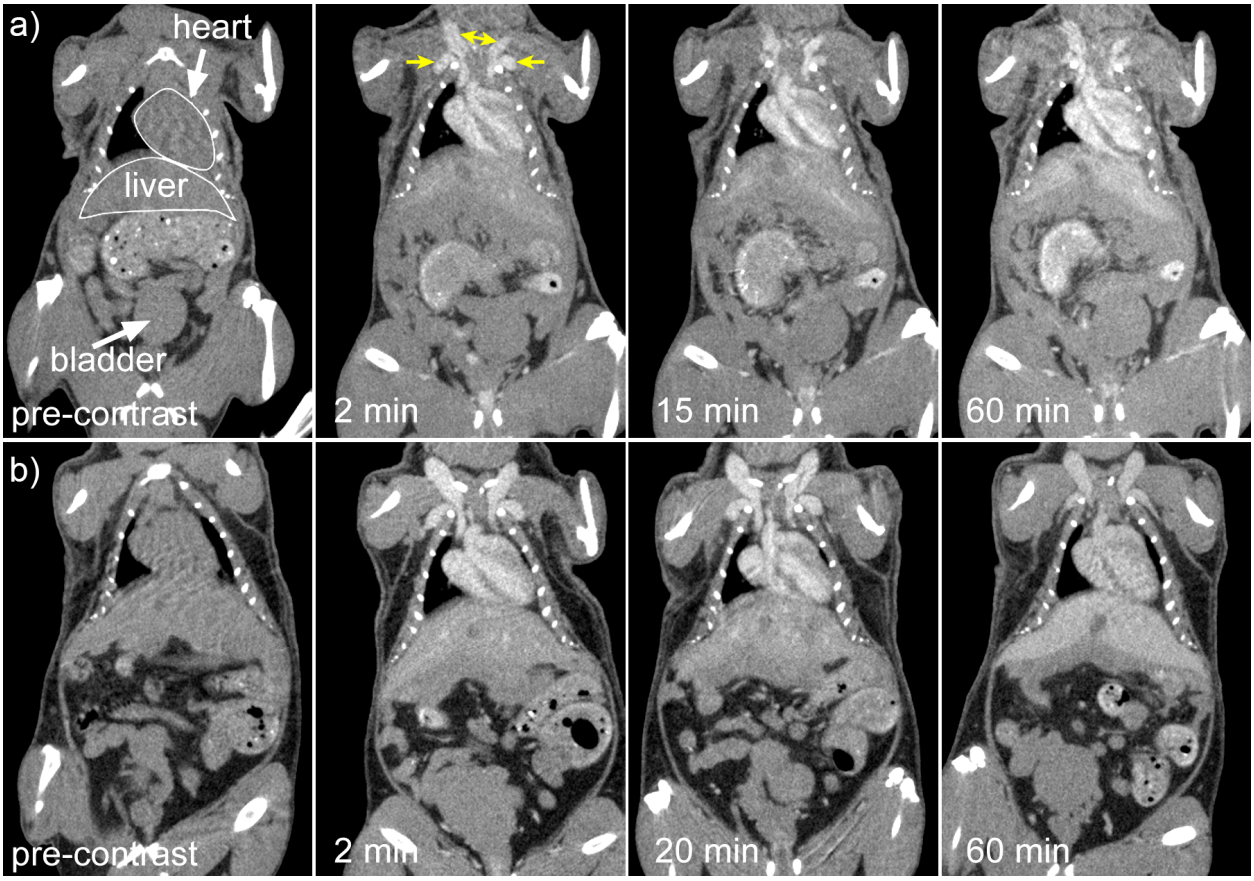

Figure 7. Representative coronal micro-CT images showing the heart, liver, aorta, jugular veins and bladder of mice that received contrast agent formulated at a) 1:1 and b) 0.5:1 PEG_{114}-PLA_{53}:ErNP mass ratios. All times are reported from the completion of the contrast agent injection. In the 2 minute image in a), the external jugular veins (double arrowheads) and the axillary veins (arrows) are clearly visible.

Quantitative analysis indicated an increase in blood pool CT number of over 250 HU compared to pre-contrast values. The bladder was indistinguishable from pre-contrast values, indicating that the agent was not cleared through the renal system, as expected of materials that exceed the size of renal fenestrations.[14] By the one-hour mark, the liver and the spleen had increased up to 180 ± 15 HU and 278 ± 18 HU, respectively, for the 1:1 formulation, confirming the hypothesis that

large nanoparticles are cleared through the MPS.[35, 36] In the myocardium, the CT number was just under 100 HU at all time points, which was expected of soft tissue in the absence of contrast material. As expected, the 0.5:1 polymer:ErNP assemblies demonstrated lower stealth activity, due to the lower amount of polymer used in the synthesis of the assembly, and were cleared from the blood more rapidly as indicated by the decreased intensity of the blood pool in the micro-CT images. Overall, this initial imaging study demonstrates that these new contrast agents can be dispersed and injected into mice at a concentration sufficient to achieve vascular contrast by micro-CT *in vivo*. Furthermore, the particles exhibited sufficient stealth properties to circulate in the vasculature for at least 1 hour. This suggests the promise of these new lanthanide-based agents for applications such as dual-energy imaging and spectral CT.

CONCLUSIONS

In this study, by systematically comparing a series of amphiphilic block copolymers composed of different hydrophobic blocks and different PEG mass fractions, we identified PEG_{114}-PLA_{53} as an amphiphilic copolymer that can encapsulate oleate-coated $NaErF_4$ nanoparticles. The PEG_{114}-PLA_{53}:ErNP assemblies redispersed into colloidally stable particles in saline after lyophilization and remained in the blood pool *in vivo* for at least an hour – a time period that well exceeds live animal micro-CT requirements. Importantly, we were able to formulate the assemblies at a high concentration of 100 mg/mL of erbium using PEG_{114}-PLA_{53}. At a delivered dose of 0.2 mL per mouse, this new contrast agent formulation resulted in the enhancement of blood pool in micro-CT images (at 80 kVp) by approximately 250 HU (above a soft tissue baseline of 100 HU) for at least an hour following contrast agent administration. This system should be readily adaptable for a variety of lanthanides, as the metal can be easily substituted in the oleate-coated $NaErF_4$ while

retaining very similar properties, suggesting its promise as a new class of contrast agents for micro-CT as well as other imaging modalities such as MRI and optical imaging, in which lanthanides are utilized. Future studies will explore further the biodistribution and toxicity profiles of these agents.

SUPPORTING INFORMATION

Additional methods, DLS data, NMR spectra, SEC traces, and time-course size measurements.

ACKNOWLEDGMENTS

The authors thank Aneta Borecki for performing SEC measurements and the cell viability assays, Jennifer Hadway for performing the tail-vein catheterizations in this work, and the Biotron Experimental Climate Change Research Centre at Western University in London for assistance with TEM and MS.

FUNDING SOURCES

Funding for this work was provided by the Heart and Stroke Foundation of Canada (grant G-14-005959). C. Cruje acknowledges support from an Ontario Graduate Scholarship. D. W. Holdsworth is the Dr. Sandy Kirkley Chair of Musculoskeletal Research. E. R. Gillies was funded in part by a Canada Research Chair in Biomaterials Synthesis. M. Drangova was supported in part by a Career Investigator Award from the Heart and Stroke Foundation of Ontario.

REFERENCES

(1) Abarbanell, A. M.; Herrmann, J. L.; Weil, B. R.; Wang, Y.; Tan, J.; Moberly, S. P.; Fiege, J. W.; Meldrum, D. R. Animal Models of Myocardial and Vascular Injury. *J. Surg. Res.* **2010**, *162*, 239-249.

(2) Camacho, P.; Fan, H.; Liu, Z.; He, J. Q. Small mammalian animal models of heart disease. *Am. J. Cardiovasc. Dis.* **2016**, *6*, 70-80.

(3) Day, C. P.; Merlino, G.; Van Dyke, T. Preclinical mouse cancer models: a maze of opportunities and challenges. *Cell* **2015**, *163*, 39-53.

(4) Xu, H.; Baldini, A. Genetic pathways to mammalian heart development: Recent progress from manipulation of the mouse genome. *Semin. Cell Dev. Biol.* **2007**, *18*, 77-83.

(5) Lancelot, E.; Amirbekian, V.; Brigger, I.; Raynaud, J. S.; Ballet, S.; David, C.; Rousseaux, O.; Le Greneur, S.; Port, M.; Lijnen, H. R.; Bruneval, P.; Michel, J. B.; Ouimet, T.; Roques, B.; Amirbekian, S.; Hyafil, F.; Vucic, E.; Aguinaldo, J. G.; Corot, C.; Fayad, Z. A. Evaluation of matrix metalloproteinases in atherosclerosis using a novel noninvasive imaging approach. *Arterioscler. Thromb. Vasc. Biol.* **2008**, *28*, 425-432.

(6) Mateo, J.; Benito, M.; Espana, S.; Sanz, J.; Jimenez-Borreguero, J.; Fuster, V.; Ruiz-Cabello, J. Magnetic Resonance Imaging of the Atherosclerotic Mouse Aorta. *Methods Mol. Biol.* **2015**, *1339*, 387-394.

(7) Ahmadi, A.; Thorn, S. L.; Alarcon, E. I.; Kordos, M.; Padavan, D. T.; Hadizad, T.; Cron, G. O.; Beanlands, R. S.; DaSilva, J. N.; Ruel, M.; deKemp, R. A.; Suuronen, E. J. PET imaging of a collagen matrix reveals its effective injection and targeted retention in a mouse model of myocardial infarction. *Biomaterials* **2015**, *49*, 18-26.

(8) Bondoc, A. B.; Detombe, S.; Dunmore-Buyze, J.; Gutpell, K. M.; Liu, L.; Kaszuba, A.; Han, S.; McGirr, R.; Hadway, J.; Drangova, M.; Hoffman, L. M. Application of 3-D echocardiography and gated micro-computed tomography to assess cardiomyopathy in a mouse model of duchenne muscular dystrophy. *Ultrasound Med. Biol.* **2014**, *40*, 2857-2867.

(9) Cherin, E.; Williams, R.; Needles, A.; Liu, G.; White, C.; Brown, A. S.; Zhou, Y. Q.; Foster, F. S. Ultrahigh frame rate retrospective ultrasound microimaging and blood flow visualization in mice in vivo. *Ultrasound Med. Biol.* **2006**, *32*, 683-691.

(10) Badea, C. T.; Drangova, M.; Holdsworth, D. W.; Johnson, G. A. In vivo small-animal imaging using micro-CT and digital subtraction angiography. *Phys. Med. Biol.* **2008**, *53*, R319-350.

(11) Poole, K. M.; Tucker-Schwartz, J. M.; Sit, W. W.; Walsh, A. J.; Duvall, C. L.; Skala, M. C. Quantitative optical imaging of vascular response in vivo in a model of peripheral arterial disease. *Am. J. Physiol. Heart Circ. Physiol.* **2013**, *305*, H1168-1180.

(12) Detombe, S. A.; Ford, N. L.; Xiang, F.; Lu, X.; Feng, Q.; Drangova, M. Longitudinal follow-up of cardiac structure and functional changes in an infarct mouse model using retrospectively gated micro-computed tomography. *Invest. Radiol.* **2008**, *43*, 520-529.

(13) Willekens, I.; Lahoutte, T.; Buls, N.; Vanhove, C.; Deklerck, R.; Bossuyt, A.; de Mey, J. Time-course of contrast enhancement in spleen and liver with Exia 160, Fenestra LC, and VC. *Mol. Imaging Biol.* **2009**, *11*, 128-135.

(14) Choi, C. H.; Zuckerman, J. E.; Webster, P.; Davis, M. E. Targeting kidney mesangium by nanoparticles of defined size. *Proc. Natl. Acad. Sci. U.S.A.* **2011**, *108*, 6656-6661.

(15) Detombe, S. A.; Dunmore-Buyze, J.; Drangova, M. Evaluation of eXIA 160 cardiac-related enhancement in C57BL/6 and BALB/c mice using micro-CT. *Contrast Media Mol. Imaging* **2012**, *7*, 240-246.

(16) Ashton, J. R.; Clark, D. P.; Moding, E. J.; Ghaghada, K.; Kirsch, D. G.; West, J. L.; Badea, C. T. Dual-energy micro-CT functional imaging of primary lung cancer in mice using gold and iodine nanoparticle contrast agents: a validation study. *PLoS One* **2014**, *9*, e88129.

(17) Jackson, A. W.; Chandrasekharan, P.; Shi, J.; Rannard, S. P.; Liu, Q.; Yang, C. T.; He, T. Synthesis and in vivo magnetic resonance imaging evaluation of biocompatible branched copolymer nanocontrast agents. *Int. J. Nanomedicine* **2015**, *10*, 5895-5907.

(18) Nazemi, A.; Martínez, F.; Scholl, T.; Gillies, E. Biodegradable dendritic polymersomes as modular, high-relaxivity MRI contrast agents. *RSC Adv.* **2012**, *2*, 7971-7973.

(19) Soleimani, A.; Martínez, F.; Economopoulos, V.; Foster, P.; Scholl, T.; Gillies, E. Polymer cross-linking: a nanogel approach to enhancing the relaxivity of MRI contrast agents. *J. Mater. Chem. B* **2013**, *1*, 1027-1034.

(20) Faucher, L.; Tremblay, M.; Lagueux, J.; Gossuin, Y.; Fortin, M. A. Rapid synthesis of PEGylated ultrasmall gadolinium oxide nanoparticles for cell labeling and tracking with MRI. *ACS Appl. Mater. Interfaces* **2012**, *4*, 4506-4515.

(21) Zhu, L.; Yang, Y.; Farquhar, K.; Wang, J.; Tian, C.; Ranville, J.; Boyes, S. G. Surface Modification of Gd Nanoparticles with pH-Responsive Block Copolymers for Use As Smart MRI Contrast Agents. *ACS Appl Mater. Interfaces* **2016**, *8*, 5040-5050.

(22) Chatterjee, D. K.; Rufaihah, A. J.; Zhang, Y. Upconversion fluorescence imaging of cells and small animals using lanthanide doped nanocrystals. *Biomaterials* **2008**, *29*, 937-943.

(23) Zhou, J.; Sun, Y.; Du, X.; Xiong, L.; Hu, H.; Li, F. Dual-modality in vivo imaging using rare-earth nanocrystals with near-infrared to near-infrared (NIR-to-NIR) upconversion luminescence and magnetic resonance properties. *Biomaterials* **2010**, *31*, 3287-3295.

(24) Budijono, S. J.; Shan, J.; Yao, N.; Miura, Y.; Hoye, T.; Austin, R. H.; Ju, Y.; Prud'homme, R. K. Synthesis of Stable Block-Copolymer-Protected $NaYF_4$:Yb^{3+}, Er^{3+} Up-Converting Phosphor Nanoparticles. *Chem. Mater.* **2010**, *22*, 311-318.

(25) Wang, M.; Abbineni, G.; Clevenger, A.; Mao, C.; Xu, S. Upconversion nanoparticles: synthesis, surface modification and biological applications. *Nanomedicine* **2011**, *7*, 710-729.

(26) Liu, Y.; Ai, K.; Liu, J.; Yuan, Q.; He, Y.; Lu, L. A high-performance ytterbium-based nanoparticulate contrast agent for in vivo X-ray computed tomography imaging. *Angew. Chem. Int. Ed.* **2012**, *51*, 1437-1442.

(27) Tse, J. J.; Dunmore-Buyze, P. J.; Drangova, M.; Holdsworth, D. W. Erbium-Based Perfusion Contrast Agent for Small-Animal Microvessel Imaging. *Contrast Media Mol. Imaging* **2017**, *2017*, 10.

(28) Li, Z.; Zhang, Y. An efficient and user-friendly method for the synthesis of hexagonal-phase NaYF(4):Yb, Er/Tm nanocrystals with controllable shape and upconversion fluorescence. *Nanotechnology* **2008**, *19*, 345606-345610.

(29) Zhao, G.; Tong, L.; Cao, P.; Nitz, M.; Winnik, M. A. Functional PEG-PAMAM-tetraphosphonate capped NaLnF(4) nanoparticles and their colloidal stability in phosphate buffer. *Langmuir* **2014**, *30*, 6980-6989.

(30) Couffin, A.; Delcroix, D.; Martín-Vaca, B.; Bourissou, D.; Navarro, C. Mild and efficient preparation of block and gradient copolymers by methanesulfonic acid catalyzed ring-

opening polymerization of caprolactone and trimethylene carbonate. *Macromolecules* **2013**, *46*, 4354-4360.

(31) Lohmeijer, B.; Pratt, R.; Leibfarth, F.; Logan, J.; Long, D.; Dove, A.; Nederberg, F.; Choi, J.; Wade, C.; Waymouth, R.; Hedrick, J. Guanidine and Amidine Organocatalysts for Ring-Opening Polymerization of Cyclic Esters. *Macromolecules* **2006**, *39*, 8574-8583.

(32) Ford, N. L.; McCaig, L.; Jeklin, A.; Lewis, J. F.; Veldhuizen, R. A.; Holdsworth, D. W.; Drangova, M. A respiratory-gated micro-CT comparison of respiratory patterns in free-breathing and mechanically ventilated rats. *Physiol. Rep.* **2017**, *5*, e13074.

(33) Aggarwal, P.; Hall, J. B.; McLeland, C. B.; Dobrovolskaia, M. A.; McNeil, S. E. Nanoparticle interaction with plasma proteins as it relates to particle biodistribution, biocompatibility and therapeutic efficacy. *Adv. Drug Delivery Rev.* **2009**, *61*, 428-437.

(34) Kim, S.; Shi, Y.; Kim, J. Y.; Park, K.; Cheng, J. X. Overcoming the barriers in micellar drug delivery: loading efficiency, in vivo stability, and micelle-cell interaction. *Expert Opin. Drug Deliv.* **2010**, *7*, 49-62.

(35) Butcher, N. J.; Mortimer, G. M.; Minchin, R. F. Drug delivery: Unravelling the stealth effect. *Nat. Nanotechnol.* **2016**, *11*, 310-311.

(36) Yang, Q.; Jones, S. W.; Parker, C. L.; Zamboni, W. C.; Bear, J. E.; Lai, S. K. Evading immune cell uptake and clearance requires PEG grafting at densities substantially exceeding the minimum for brush conformation. *Mol. Pharmacol.* **2014**, *11*, 1250-1258.

(37) Naccache, R.; Vetrone, F.; Mahalingam, V.; Cuccia, L.; Capobianco, J. Controlled synthesis and water dispersibility of hexagonal phase $NaGdF_4$:Ho^{3+}/Yb^{3+} nanoparticles. *Chem. Mater.* **2009**, *21*, 717-723.

(38) Schubert, S.; Delaney, J. J.; Schubert, U. Nanoprecipitation and nanoformulation of polymers: from history to powerful possibilities beyond poly(lactic acid). *Soft Matter* **2011**, *7*, 1581-1588.

(39) Redhead, H. M.; Davis, S. S.; Illum, L. Drug delivery in poly(lactide-co-glycolide) nanoparticles surface modified with poloxamer 407 and poloxamine 908: in vitro characterisation and in vivo evaluation. *J. Controlled Release* **2001**, *70*, 353-363.

(40) Kamaly, N.; Yameen, B.; Wu, J.; Farokhzad, O. C. Degradable Controlled-Release Polymers and Polymeric Nanoparticles: Mechanisms of Controlling Drug Release. *Chem. Rev.* **2016**, *116*, 2602-2663.

(41) Curia, S.; Howdle, S. Towards sustainable polymeric nano-carriers and surfactants: facile low temperature enzymatic synthesis of bio-based amphiphilic copolymers in $scCO_2$. *Polym. Chem.* **2016**, *7*, 2130-2142.

(42) Pombo Garcia, K.; Zarschler, K.; Barbaro, L.; Barreto, J. A.; O'Malley, W.; Spiccia, L.; Stephan, H.; Graham, B. Zwitterionic-coated "stealth" nanoparticles for biomedical applications: recent advances in countering biomolecular corona formation and uptake by the mononuclear phagocyte system. *Small* **2014**, *10*, 2516-2529.

(43) Manolova, V.; Flace, A.; Bauer, M.; Schwarz, K.; Saudan, P.; Bachmann, M. F. Nanoparticles target distinct dendritic cell populations according to their size. *Eur. J. Immunol.* **2008**, *38*, 1404-1413.

(44) Basu Ray, G.; Chakraborty, I.; Moulik, S. P. Pyrene absorption can be a convenient method for probing critical micellar concentration (CMC) and indexing micellar polarity. *J Colloid Interface Sci.* **2006**, *294*, 248-254.

For Table of Contents Use Only